# Thermodynamics of Mercury Porosimetry and Effective Surface Area of Hardened Cement Pastes

H. Utsumi[1], S. Tada[2]
[1]*Chiba Institute of Technology, Chiba, Japan,* [2]*Texte, Inc., Tokyo, Japan*

## 1. Introduction

Mercury intrusion porosimetry (MIP) is a useful technique in characterizing the microstructural parameters of porous materials, such as porosity, pore size distribution, specific surface area. In the previous microstructural investigation applied to cement-based materials, MIP has been carried out by various authors from different point of view [1-4] where pore radius played a central role.

MIP experiments primarily provide the relationship between pressure and mercury volume intruded into the pore space, and so the intrusion and extrusion processes can be obtained. In the standard procedure of MIP, Washburn equation [5] is applied to determine the pore size distribution and specific surface area. Assuming cylindrical pore shape (Eq.1), it gives,

$$P_m = -\frac{2\Phi_m \cos\theta_m}{r} \tag{1}$$

where, $r$ is radius of the cylindrical pore, $P_m$ is applied pressure, $\Phi_m$ is surface tension of mercury, $\theta_m$ is contact angle between liquid mercury and solid pore surface. Washburn equation can calculate radius of pore from pressure and widely used as the standard MIP practice, however, we have no theory that can directly correlate pressure and intruded mercury volume without assuming any pore geometry though some theoretical developments have been made [6-8].

In this study, we developed a new theory for MIP, which is formulated from the equation of state on the basis of rigorous thermodynamics. To formulate the equation of state of mercury in porous body, a thermodynamics system consisting only of mercury of vapor and liquid phases was assumed whereas the porous media is represented with each interfacial free energy.

The system corresponds to an actual MIP procedure, and can be described by the differential Helmholtz free energy with component of interfacial energies related to the liquid mercury and vapor-phase mercury in pore spaces under increasing pressure. This formulation takes into account the condensation and evaporation of vapor phase mercury in pores. In addition, neither particular pore geometry nor the relative arrangements of mercury in the pore spaces are assumed.

In an isothermal equilibrium condition, and introducing Young's equation, the equation of state can be presented with a new concept of the effective surface area comprised of interfaces of each phase in the thermodynamic system. The physical meaning of the effective surface area is the sum of

interfacial areas changing with an increase or decrease in pressure. When mercury fills entire pore space, the effective surface area yields a specific surface area. In this paper, characteristics of the effective surface area associated with intrusion process is demonstrated with hardened cement paste specimens of various water cement ratios and compared with experimental results obtained with other methods.

## 2. Thermodynamics of mercury porosimetry

### 2.1 Definition of thermodynamic system

The thermodynamics system is shown in (Fig. 1), where the system consists of mercury and solid and modeled to represent the actual MIP procedure. The system is a closed isothermal system consisting of three phases: inert incompressible porous solid (*s*), liquid mercury (*l*) and vapor-phase mercury (*g*). It is assumed that the vapor-phase mercury (*g*) fills the pore space other than that filled with liquid mercury. We assumed no particular pore geometry or the relative arrangements of mercury in the pore spaces. Furthermore, the liquid-phase mercury is distinguished regarding whether it is within or outside the pore space. Gravitational effects are neglected.

### 2.2 Equation of state of mercury in porous body

The total differential of Helmholtz free energy d*F* characterizing the entire system is given by

$$\begin{aligned} dF = &-SdT + P_l^o dV_l^o + P_l^i dV_l^i + P_g^i dV_g^i \\ &+ \Phi_{sg} dA_{sg} + \Phi_{lg} dA_{lg} + \Phi_{sl} dA_{sl} \end{aligned} \tag{2}$$

where $P$ is the pressure, $V$ and $A$ are the volume of mercury and interfacial area, respectively, $S$ is entropy, $T$ is absolute temperature and $\Phi$ is surface tension. The subscripts *lg*, *sl* and *sg* denote the interfaces of each phase, while superscripts *i* and *o* denote the location interior and exterior of the pore space, respectively.

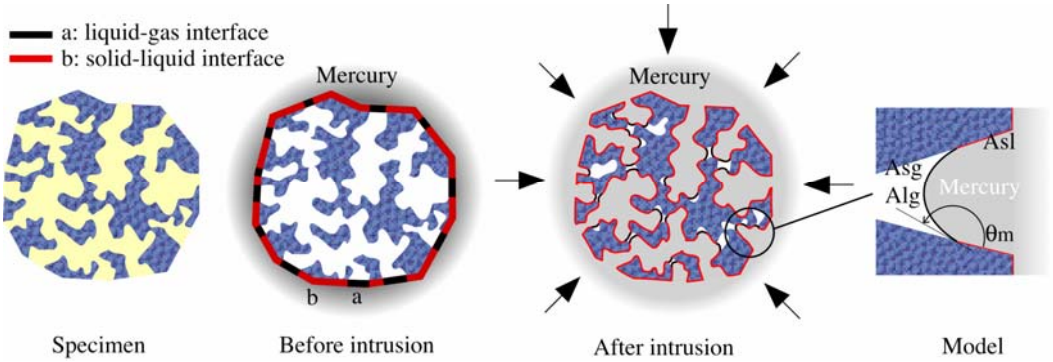


Fig. 1 The thermodynamics system

Because the isothermal equilibrium condition requires d$F$ and d$T$ to be zero, (Eq.2) reduces to

$$P_l^o dV_l^o + P_l^i dV_l^i + P_g^i dV_g^i + \Phi_{sg} dA_{sg} + \Phi_{lg} dA_{lg} + \Phi_{sl} dA_{sl} = 0 \quad (3)$$

The interfacial energy balance of liquid mercury in the interior pore spaces requires the Young's equation with the equilibrium contact angle $\theta_m$ between lg and sl interfaces

$$\Phi_{lg} \cos\theta_m + \Phi_{sl} = \Phi_{sg} \quad (4)$$

where, $\Phi_{lg}$ denotes the surface tension corresponding to $\Phi_m$ in (Eq.1). Substituting (Eq.4) into (Eq.3) gives

$$(P_l^o dV_l^o + P_l^i dV_l^i + P_g^i dV_g^i) + \Phi_m (dA_{lg} - dA_{sl} \cos\theta_m) + \Phi_{sl} (dA_{sg} + dA_{sl}) = 0 \quad (5)$$

Here, assuming that the volume of liquid phase mercury, volume of pore space and specific surface area of the porous solid are constant during MIP processes, the following relations can be derived,

$$dV_l^i + dV_l^o = 0 \quad (6)$$

$$dV_l^i + dV_g^i = 0 \quad (7)$$

$$dA_{sg} + dA_{sl} = 0 \quad (8)$$

Substituting (Eq.6) - (Eq.8) into (Eq.5) gives,

$$(P_l^i - P_l^o - P_g^i) dV_l^i + \Phi_m (dA_{lg} - dA_{sl} \cos\theta_m) = 0 \quad (9)$$

where, $P^i_l = P^o_l = P^i_g$ can be held at the equilibrium isothermal condition, and $P_m$ and $V_m$ can be defined as intrusion pressure and intruded volume of the actual MIP process, respectively, then the left side term of (Eq.9) reduces to,

$$(P_l^i - P_l^o - P_g^i) dV_l^i = -P_m dV_m \quad (10)$$

Finally, we can obtain a differential form of the Helmholtz free energy of the thermodynamics system representing the MIP process as

$$-P_m dV_m + \Phi_m (dA_{lg} - dA_{sl} \cos\theta_m) = 0 \tag{11}$$

The definite integration of (Eq.11) regarding $V_m$ from 0 to $V_m$, $A_{lg}$ from an initial value *a* to $A_{lg}$ and $A_{sl}$ from an it initial value *b* to $A_{sl}$ yields,

$$-P_m \int_0^{V_m} dV_m + \Phi_m (\int_a^{A_{lg}} dA_{lg} - \cos\theta_m \int_b^{A_{sl}} dA_{sl}) = 0 \tag{12}$$

where *a* and *b* can be negligible with respect to $A_{lg}$ as shown in (Fig. 1). Finally, the equation of state (Eq.2) is expressed in the following algebraic equation.

$$\Phi_m (A_{lg} - A_{sl} \cos\theta_m) = P_m V_m \tag{13}$$

We introduce the effective surface area *A*', defined by

$$A' = (A_{lg} - A_{sl} \cos\theta_m) \tag{14}$$

The effective surface area represents actually covered pore surfaces with mercury associated with changes in pressure, and (Eq.13) is a complete equation of state of mercury in porous media compared to the Washburn equation that lacks volume component.

2.3 Characteristics of the effective surface area

When the entire pore space is completely filled with mercury, the contact angle $\theta_m$ will approach to $\pi$ (180°) and $A_{lg}$ converges to zero. Then, the effective surface area (Eq.14) reduces to

$$(A_{lg} - A_{sl} \cos\theta_m) = 0 - A_{sl} \cos(\pi) = A_{sl} \tag{15}$$

where $A_{sl}$ is regarded as the entire surface area of the pore surfaces. Thus, at the complete mercury intrusion, the effective surface area is equal to the specific surface area such that measured with the BET theory at the monolayer gas adsorption.

When the pore geometry is assumed to be cylindrical with a radius *r* and length *L* (Eq.13) is expressed as

$$P_m = \frac{(A_{lg} - A_{sl} \cos\theta_m)}{V_m} \Phi_m = \frac{-A_{sl} \cos\theta_m}{V_m} \Phi_m = -\frac{2\pi r L \cos\theta_m}{\pi r^2 L} \Phi_m = -\frac{2\Phi_m \cos\theta_m}{r} \tag{16}$$

Therefore, the Washburn equation (Eq.1) is a special case of the equation of state for mercury in porous media derived as (Eq.13).

3. Experimental results

3.1 Experimental conditions

Samples of hardened cement paste were prepared with different water cement ratios of 0.3 to 0.5. These were cured in plastic bag for 400 days at a constant temperature of 20°C, and dried in an oven (105°C) until a constant weight was attained.

The sample size was 0.4 mm to 0.28 mm throughout, corresponding to a maximum mass of approximately 0.25 g.

Mercury intrusion was performed with a maximum intrusion pressure of 400 MPa. An automatic pressure control was employed in each test taking approximately 180 minutes.

Furthermore, to compare the characteristics of effective surface area, water vapor adsorption isotherms were measured with the same specimen using a volumetric technique. Prior to the sorption measurement, sample was subjected to oven-dry at 105 °C which is a milder drying than D-dry. The drying condition may affect the specific surface areas when water is used as an adsorbete while nitrogen may pose no effect on the result.

3.2 Total porosity

The direct consequence of MIP is shown in (Fig. 2), where the relationships between pressure and cumulative volume of mercury at different water cement ratios are shown. It can be seen that total cumulative volume increases with an increase in water cement ratio.

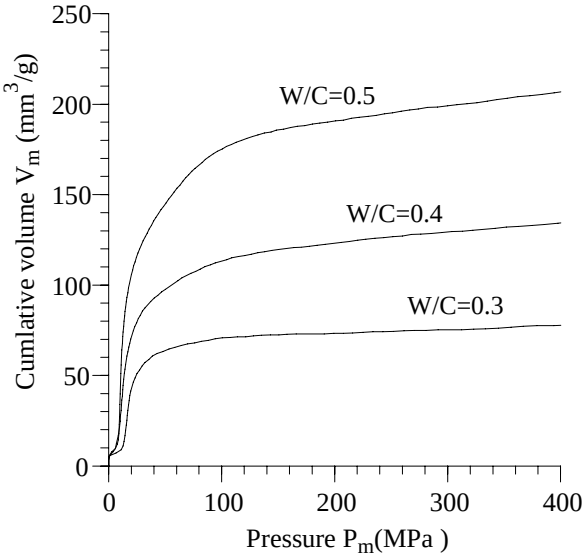


Fig. 2 Relationship between pressure and cumulative volume

Total porosity measured with MIP and other methods is shown in (Fig. 3). The MIP total porosity at a maximum pressure of 400 MPa was smaller than that of theoretical total porosity calculated with Powers' formula and

much smaller than water-filled porosity based on the oven-dry condition at 105°C [9]. Obviously in hardened cement pastes, there is a space available only to water molecules and inaccessible to $N_2$ and mercury. In the subsequent discussion, the total porosity of hardened cement paste is defined as that available to any fluids, e.g. MIP total porosity at a pressure of 400 MPa. Specific surface area to be measured with MIP will be based on this definition.

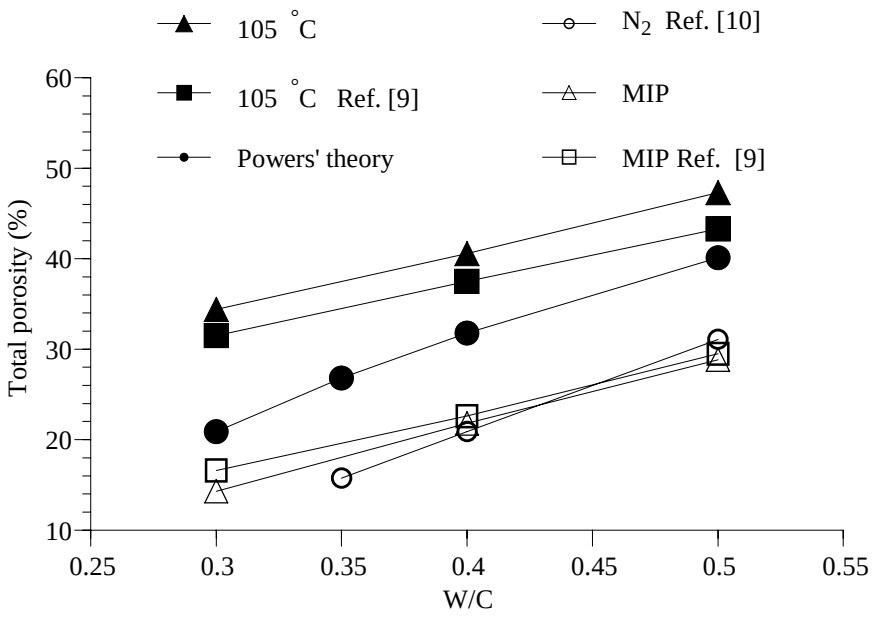


Fig. 3 Total porosity of hardened cement pastes measured with various fluids

4. Pore structure analysis with the effective surface area

4.1 Pore size distribution

The effective surface area can be measured inclusive of contact angle $\theta_m$ and it is not necessary to know $\theta_m$ prior to the MIP experiment. Introducing the effective hydraulic radius $R_h$ of (Eq.17) using the effective surface area, the measured MIP data is more directly shown as pore size distribution than using Washburn equation that assumes cylindrical pore geometry.

$$R_h = \frac{V_m}{A_{lg} - A_{sl}\cos\theta_m} \tag{17}$$

The pore size distribution of hardened cement pastes with effective surface area and effective hydraulic radius is shown in (Fig. 4).

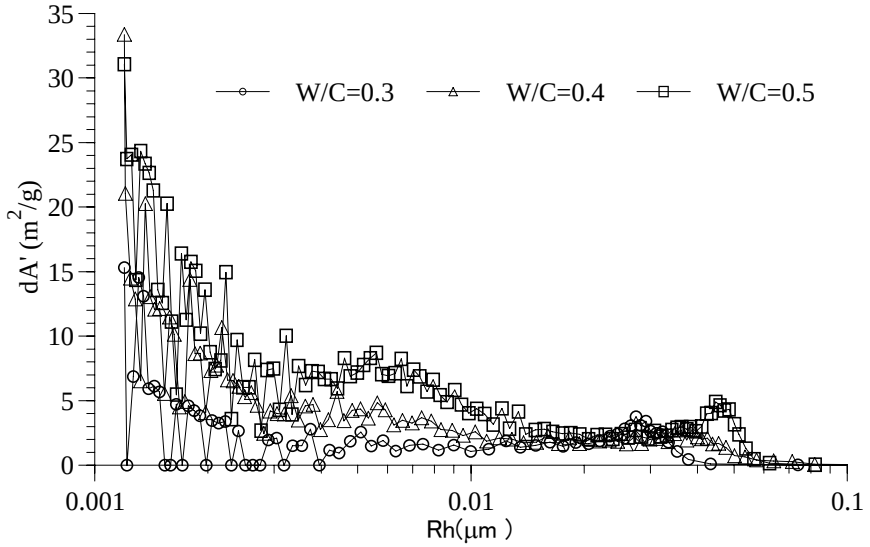


Fig. 4 Pore size distribution of hardened cement pastes using effective surface area

4.2 Fractal dimension

Surface fractal dimension is a non-integer number representing complexity of the surface of materials and recently ranked one of the microstructural parameters of porous solid. Pfiefer and Avnir presented for the first time an unified treatment of specific surface area and its measurement methods in terms of fractal dimension [11]. Winslow showed the first results of surface fractal dimension (between 2 and 3) of hardened cement paste by small angle X-ray scattering method. It was almost 3 regardless of the water-cement ratio and he concluded that the surface of hardened cement paste is highly complex [12].

Fractal dimension obtainable from MIP data can be expressed, with volume $V$ and radius $r$, as $V \propto r^{(3\text{-}D)}$ or its differential form $dV/dr \propto r^{(2\text{-}D)}$ [13]. In this study, surface fractal dimension was calculated using effective surface area $A$' and hydraulic radius $R_h$ as follows,

$$A' \propto R_h^{(2-D)} \tag{18}$$

Plotting $A$' and $R_h$ in log scale in (Fig. 5), a good linearity was observed at a region r< 0.01 micrometer where the gradient gives a fractal dimension. Fractal dimension of hardened cement paste was almost 3 regardless of water-cement ratio and shows agreement with the conclusion of Winslow. However, Fractal dimension of hardened cement paste obtained by other methods, such as water vapor adsorption [14], small angle neutron scattering [15] or another study with small angle X-ray scattering [16] showed 2.5-2.6 without exception suggesting a need of further investigation.

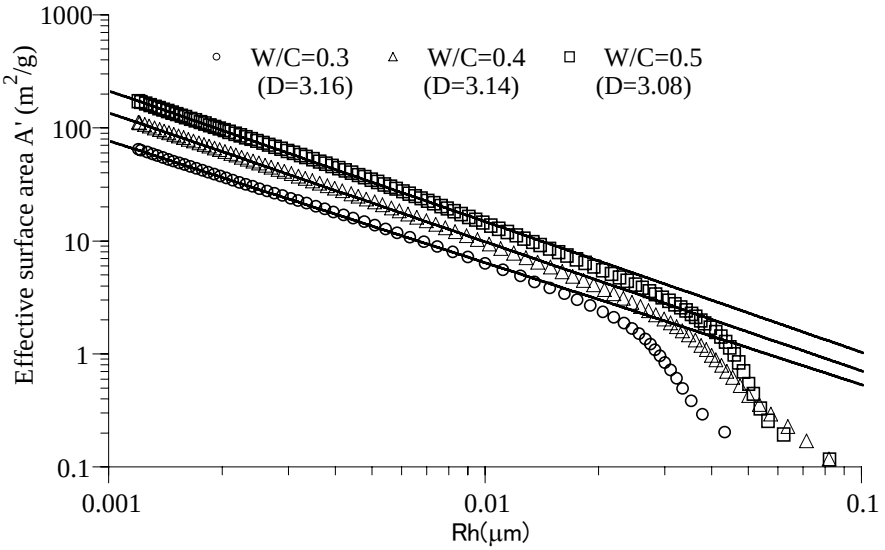


Fig. 5 Fractal dimensions of hardened cement pastes obtained with MIP

4.3 Specific surface area

Assuming that mercury fills entire pore space at the maximum pressure in this experiment (400MPa), we can determine the specific surface area from the effective surface area with (Eq.15). On the other hand, application of the Rootare-Prenzlow equation to MIP data can also provide specific surface area as follows,

$$S_{R.P.} = \frac{1}{\left|\cos\theta_m \, \Phi_m\right|} \int_0^V P_m dV_m \tag{19}$$

Specific surface area $S_{R.P.}$ of (Eq.19) can be calculated through the numerical integration of MIP data with a contact angle of $\theta_m$=141° and $\Phi_m$ of $480 \times 10^{-3}$ N/m. From the water vapor adsorption isotherm, the specific surface area was determined using the BET theory with a value of 0.125 $nm^2$ for the area covered by a gas molecule. The effective surface area and specific surface areas determined with various methods are shown in (Fig. 6).

With change in W/C, the effective surface areas generally shows similar tendency with other methods and similar result with BET surface area using water. Because specific surface area measurement is highly sensitive to the specimen pre-treatment such as drying condition, the oven-dry at 105°C adopted in this measurement may result in a lower specific surface area than that measured with D-dried specimen that often show approximately 200 $m^2$/g regardless of its water-cement ratio [10].

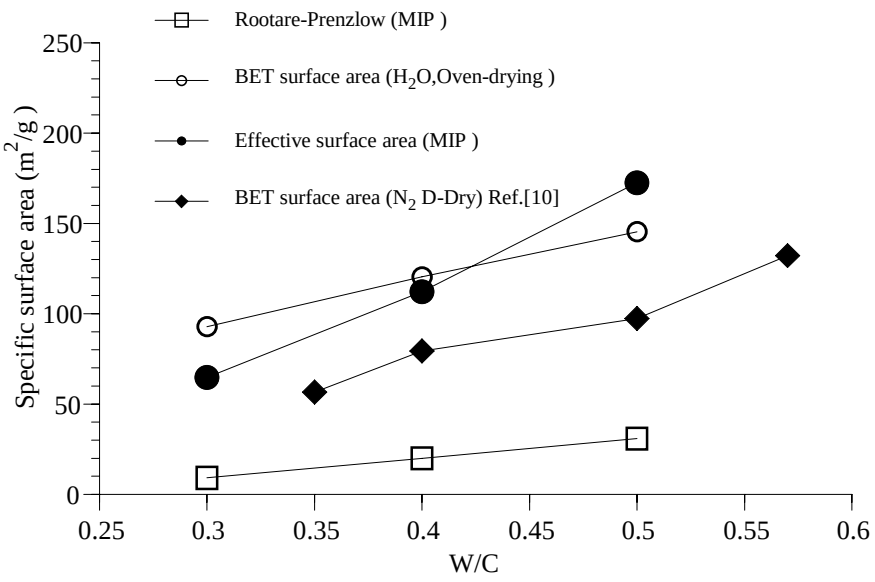


Fig.6 Effective surface area and specific surface areas determined with various methods

## 5. Conclusion

The effective surface area, capable of describing various pore structural parameters out of MIP data, was formulated from the equation of state based on rigorous thermodynamics. The equation of state of mercury consists of interfaces of each phase in the thermodynamic system and it takes into account the vapor phase transfer of mercury into pores.

In this derivation, no particular pore geometry or the relative arrangement of the filling of mercury in the pore spaces was assumed. When mercury fills the entire pore space available to mercury, the effective surface area reduced to the specific surface area, and when assuming the cylindrical geometry, the Washburn equation can be derived as a special case of the equation of state of mercury.

The effective surface area can be obtained directly form the MIP experiment as a quantity inclusive of contact angle. Thus, there is no need of determining the controversial contact angle prior to an experiment. Rootare-Prenzlow equation is useful as it does not assume any perticular pore geometry while contact angle is still needed to determine spacific surface area and hence the resulting specific surface area may be much less than that with other methods.

MIP results on a material have been used in comparison with those on other materials and lack a basis capable of being compared with those with other methods. The concept of effective surface area and the equation of state for mercury in porous body proposed in this study can be expected not only to determine various pore structural parameters but to

lead to a more accurate determination through the comparison with those with other methods.

Bibliography

[1] R. A. Cook, K. C. Hover, Mercury porosimetry of hardened cement pastes, Cement and Concrete Research 29 (1999) 993-943
[2] O. A. Kayyali, Porosity of concrete in relation to the nature of the paste-aggregate interface, Mater. Struct., 20 (115) (1987) 19-26
[3] R. Kumar, Porosity, pore size distribution and in situ strength of concrete, Cement and Concrete Research 33 (2003) 155-164
[4] R. Kumar, B. Bhattacharjee, Assessment of permeation quality of concrete through mercury intrusion porosimetry, Cement and Concrete Research 34(2004) 321-328
[5] E. W. Washburn, The dynamics of capillary flow, Physical Review 17 (3) (1921) 273-283
[6] H. M. Rootare, C. F. Prenzlow, Surface area from mercury porosimetry measurements, J. Phys. Chem. 71 (8) (1967) 2733-2735
[7] O. Kadlec, The general equation of high pressure mercury porosimetry, Adsorption Science and Technology, 1 (1984) 177-182
[8] J. Mitteldorf, G. Wilemski, Film thickness and distribution of electrolyte in porous fuel cell components, J. Electrochem. Soc., 131 (8) (1984) 1784-1788
[9] C. V. Galle, Effect of drying on cement-based materials pore structure as idntified by mercury intrusion porosimetry. A comparative study between oven-, vacuum- and freeze-drying, Cement and Concrete Research, 31 (10) (2001) 1467-1477
[10] R. Sh. Mikhail, S. A. Selim, Adsorption of Organic Vapors in relation to the pore structure of hardened Portland cement pastes, Highway Research Board Special Report 98 (1966)123-134
[11] P. Pfeifer, D. Avnir, Chemistry of noninteger dimensions between two and three. 1. Fractal theory of heterogeneous surfaces, J. Chem. Phys. 79 (7) (1983) 3558-3565
[12] D. N. Winslow, The fractal nature of the surface of cement paste, Cement and Concrte Research, 15 (1985) 817-824
[13] B. Sahouli, S. Blacher, R.Pirard, and F. Brouers, Fractal Analysis of Mercury Porosimetry Data in the Framework of the Thermodynamic Method, J Colloid Interface Sci. 214 (2) (1999) 450-454
[14] G. A, Niklasson, Adsorption on fractal structures: Application to cement materilas, Cement and Concrte Research, 23 (1993) 1153-1158
[15] F. Häußler, S. Palzer, A. Eckart, Nanostructural Investigations on Carbonation of Hydrating Tricalcium Silicate by Small Angle Neutron Scattering, LACER No. 5 (2000), Universität Leipzig
[16] R. E. Beddoe, K. Lang, Effect of moisture on fractal dimension and specific surface of hardened cement paste by small-angle X-ray scattering, Cement and Concrete Research, 24 (4) (1994) 605-612